Friction

Research Article

Role of friction in tribofilm formation: Tribochemical evolution of proteins under AFM single-asperity friction

Jiachen Chen, Heng Liu, Yu Yan✉

Cite this article: Chen JC, Liu H, Yan Y. *Friction* 2025, **13**(12): 9441073. https://doi.org/10.26599/FRICT.2025.9441073

ABSTRACT: Recent studies have indicated that tribochemical reaction layers form on metal-on-metal-bearing surfaces, which may play a significant role in the performance and longevity of artificial joints. The purpose of this study was to determine the role of friction in the formation of tribofilms, and an *in situ* atomic force microscopy single-asperity sliding setup was used to perform *in situ* microscopic friction experiments to control the contact area and load. Time-of-flight secondary ion mass spectrometry and Raman spectroscopy were also employed to investigate changes in the composition and structure of the proteins at different sliding cycles. The results revealed that the proteins first unfolded under shear and then underwent chain breakage, dehydrogenation, and desulfurization over time as friction progressed. Finally, the carbonaceous fragments did not show graphitization trends under only shear stress.

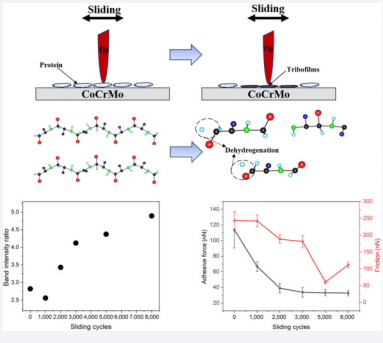

KEYWORDS: atomic force microscopy (AFM); friction; tribofilm; protein; tribochemical reactions

1 Introduction

Total hip replacement is the most efficient surgical procedure for treating end-stage arthritis and joint function loss. Over 1 million artificial joint replacements are conducted worldwide every year, with the global artificial joint market expected to reach US$25.31 billion by 2025 [1, 2]. Metallic biomaterials are commonly used as load-bearing components in artificial joints because of their excellent mechanical properties and high resistance to wear and corrosion [3–5]. However, metal materials undergo tribocorrosion degradation *in vivo* [6]. The metal ions and debris generated during wear and the corrosion of metal materials can lead to periprosthetic tissue reactions, osteolysis, and late aseptic loosening [7, 8], resulting in significantly higher failure rates than expected [9, 10].

Wimmer et al. [11, 12] observed the presence of a tribofilm on the surface of retrieved metal-metal (MoM) joints and reported that joints with a tribofilm did not experience excessive wear. Tribofilms consisting of a carbonaceous tribochemical reaction layer derived from proteins in joint fluid have also been observed in *in vitro* studies and were found to increase corrosion resistance while reducing wear and friction [13–15]. Therefore, the presence of a tribofilm may be the key to well-functioning MoM joints. Liao et al. [16] investigated a tribofilm on the surface of recycled MoM joints and observed a graphite structure. However, *in vitro* studies by Hesketh et al. [17] demonstrated that the triofilm on the MoM joint surface did not have a graphitic structure and existed in an amorphous state. This difference was possibly due to the different environmental and experimental conditions *in vivo* and *in vitro*. Therefore, the specific processes and reactions involved in this transformation are poorly understood. Mechanical shear and electrochemical corrosion are widely recognized as key factors in friction film formation, and studies have shown that carbonaceous films can form on the surfaces of alloys containing molybdenum after a specific potential is applied to the alloy in a protein solution [18]. However, few studies have focused on the effect of shear stress on tribofilm formation, especially on the evolution of protein composition and structure at the friction interface.

Most studies investigating tribofilms involve large macroscopic contacts, where the wear and loading are never uniform, only a small portion of the nominal contact area is actually in contact, and the microconvexity of the instantaneous contact changes over time as friction progresses [12, 13, 19]. This could be attributed to observations conducted at the micrometer scale, as nominally smooth surfaces will exhibit rough and uneven surfaces with concavity, convexity, and varying heights and sizes in contact at different rates and times under different stresses. Therefore, it is critical to study the behavior of single asperities with controlled geometries in continuous contact during friction. Atomic force microscopy (AFM) allows for single-asperity contact between two different interfaces, which can be used to monitor surface morphology at the nanoscale and simultaneously determine friction and adhesion forces [20]. This method of controlling the

Beijing Advanced Innovation Center for Materials Genome Engineering, Corrosion and Protection Center, Institute for Advanced Materials and Technology, University of Science and Technology Beijing, Beijing 100083, China.

✉ Corresponding author. E-mail: yanyu@ustb.edu.cn

Received: February 5, 2024; Revised: August 14, 2024; Accepted: January 22, 2025

single-asperity contact geometry, loading, and environment may be beneficial for studying the details of tribochemical reactions at the frictional interfaces of metallic biomaterials.

This study aimed to investigate the compositional changes in proteins under shear stress, and *in situ* microscopic friction experiments were performed via AFM to control the contact area and load. After the friction experiments, the adhesion and friction changes in the protein layer were measured at the friction interface, and friction interface component analysis was performed via time-of-flight secondary ion mass spectrometry (TOF-SIMS) and Raman spectroscopy. The evolution of protein molecules at the friction interface was investigated, along with the relationship between the protein layer composition and friction performance.

2 Materials and methods

2.1 Preparation of materials

The substrate material used in this study consisted of forged HC CoCrMo (ASTM F1537-11), with a chemical composition of 28.32 wt% Cr, 5.43 wt% Mo, ~0.2 wt% C, and a Co balance. The CoCrMo alloy was cut into samples 10 mm × 10 mm × 1 mm in size, and the samples were ground with SiC paper up to 5,000 grit and polished with a 0.04 μm colloidal silica slurry to achieve a flat surface with approximately 1 nm roughness. After polishing, the samples were rinsed in deionized water, sonicated in ethanol, and then dried in air. Once cleaned, 50 μL of protein mixture was added to the surface, and the samples were air-dried to form a protein layer on the surface. The protein mixture was subsequently prepared by dissolving 10 wt% powdered bovine serum albumin (BSA; Shanghai Wokai Chemical Reagent Co., Ltd., China) in ultrapure water.

2.2 AFM measurements

Figure 1 presents a schematic of the *in situ* AFM sliding experiments, which were performed via an AFM (Agilent 5500, Agilent Technologies 75c, USA) with a wear-resistant diamond-like carbon (DLC)-coated silicon probe (Multi75DLC, Budget Sensors, Bulgaria) to characterize the surface properties and measure the friction force and adhesive force of the friction areas. The normal and lateral force constants of the cantilevers (k_n and k_l) were calibrated via the Sader method [21, 22]. The normal force deflection sensitivity (S_n) was calculated from the slope of the force–displacement (FD) curve [23], and the lateral force deflection sensitivity (S_l) was calculated from the slope of the static friction vs. distance curve [24]. After completing the above calibration procedure, the normal and lateral forces were calculated via Eqs. (1) and (2):

$$F_{\mathrm{n}} = k_{\mathrm{n}} S_{\mathrm{n}} V_{\mathrm{n}} \tag{1}$$

$$F_{\mathrm{l}} = k_{\mathrm{l}} S_{\mathrm{l}} V_{\mathrm{l}} \tag{2}$$

where V_{n} is the normal setpoint voltage and V_{l} is the lateral voltage signal.

In situ AFM sliding experiments were conducted in contact mode. For the wear procedure, seven 10 μm × 10 μm (64 pixels × 64 pixels) areas were scanned 100, 500, 1,000, 2,000, 3,000, 5,000,

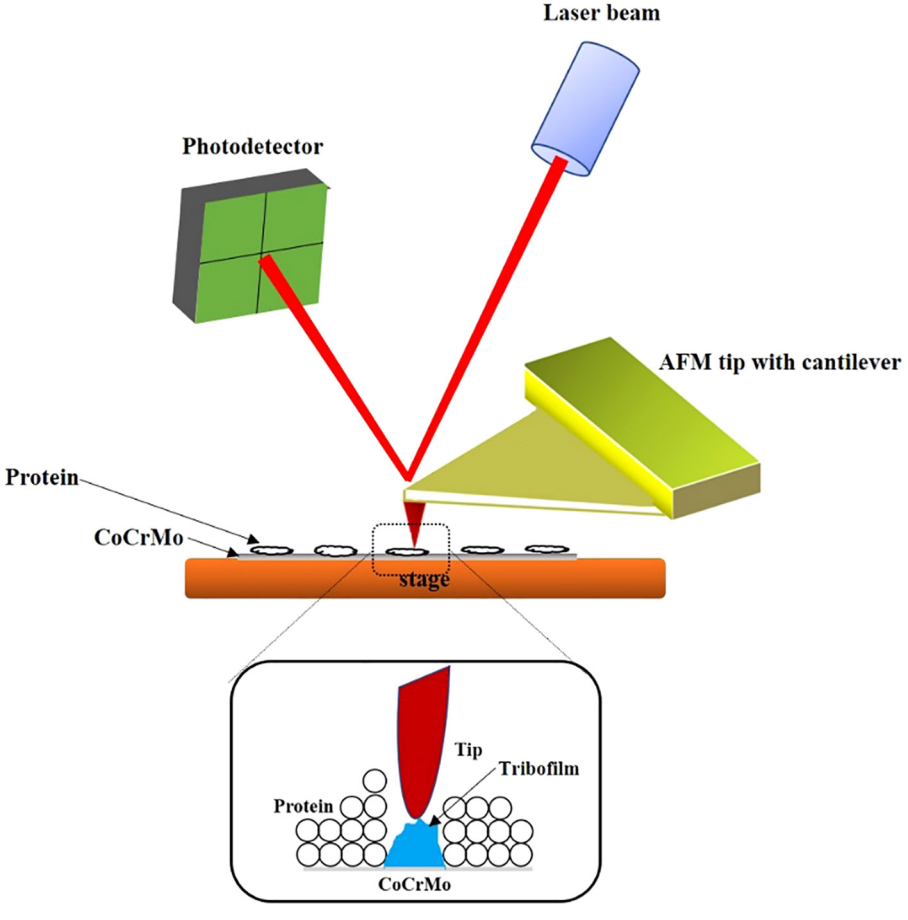

Fig. 1 Schematic of the *in situ* AFM sliding tests.

and 8,000 times with a normal force of 600 nN and a scanning rate of 10 Hz (200 μm/s). The scanning angle was set to 90° (perpendicular to the long axis of the cantilever beam) to obtain the friction image (lateral voltage signal), with one complete AFM scan process counted as one cycle. We subsequently acquired height images for every wear area in the range of 10 μm × 10 μm (256 pixels × 256 pixels) with a lower load (100 nN) and a scanning rate of 1 Hz. The adhesive force was also measured from the FD curves for different sliding cycle areas, and the FD curves were measured at least three different points on the surface of each area to determine the average value of the adhesive force.

2.3 Raman spectra

A high-resolution Raman spectrometer (LabRAM HR Evolution, HORIBA Jobin Yvon, Japan) was used to determine the structural information of the BSA molecules with different numbers of friction cycles. The excitation wavelength was 532 nm, and the power was set to 50 mW, with a detection range of 400–3,200 cm^{-1}.

2.4 Time-of-flight secondary ion mass spectrometry analysis

The chemical composition and thickness of the friction areas were analyzed via a ToF-SIMS (TOF-SIMS 5-100, ION-TOF GmbH, Germany). A second beam of pulsed 30 keV Bi+ primary ions at a 45° incidence angle to the sample surface was used to record the depth profiles and associated mass spectra. An ion dose density of approximately 10^{12} ions/cm^2, corresponding to static mode, and a current of approximately 0.5 pA were applied to all measurements. Negative secondary ion spectra, including those of C^-, H^-, O^-, S^-, CH^-, C^{2-}, and C_2H^-, were acquired from the 50 μm × 50 μm wear area.

3 Results and discussion

3.1 Surface morphology

Figure 2 shows the wear images of the protein layer under different numbers of sliding cycles. The contrast of optical microscopy (Fig. 2(a)) demonstrated obvious wear traces in the 5,000- and 8,000-cycle regions, whereas other regions were difficult to distinguish from the substrate. Figures 2(b) and 2(c) show the AFM morphology and corresponding cross-sectional profiles for the different sliding cycle regions, respectively, with the surface roughness obtained from the AFM data shown in Fig. 2(d). Overall, the wear of the protein layer increased with increasing number of sliding cycles. Initially, the surface of the protein layer was very flat, and the roughness was only approximately 0.2 nm. However, between 100 and 1,000 cycles, the surface fluctuations became obvious, and the surface roughness gradually increased to approximately 2 nm and remained stable until 3,000 cycles. At 5,000 cycles, the surface became flat again, and the roughness decreased to 0.7 nm, which was possibly related to the change in surface properties. After a further increase in the number of sliding cycles to 8,000, the protein layer broke down, and the surface roughness dramatically increased to 10.5 nm.

3.2 Friction and adhesion measurements

After the wear process, the friction and adhesive forces of the wear areas with different numbers of sliding cycles were measured. Figure 3 shows the variations in friction and adhesion force with increasing number of sliding cycles, where both friction and adhesion gradually decreased with increasing number of sliding cycles. The difference was that the adhesion force gradually decreased with sliding over the first 2,000 cycles, and then the change stabilized until 8,000 cycles. However, friction decreased between 3,000 and 5,000 cycles and increased after 8,000 cycles.

In the first 2,000 cycles, the decrease in friction was affected mainly by the surface adhesion property. The adhesion force decreased with the destruction of the protein structure, and the friction force also decreased accordingly. After the first 2,000 cycles, the adhesion force remained very stable, so the change in friction force was influenced mainly by the surface composition and properties. The significant decrease in friction at 5,000 cycles was possibly related to the generation of lubricating surfaces. In comparison, the increase in friction after 8,000 cycles could be attributed to the destruction of the protein layer and the increase

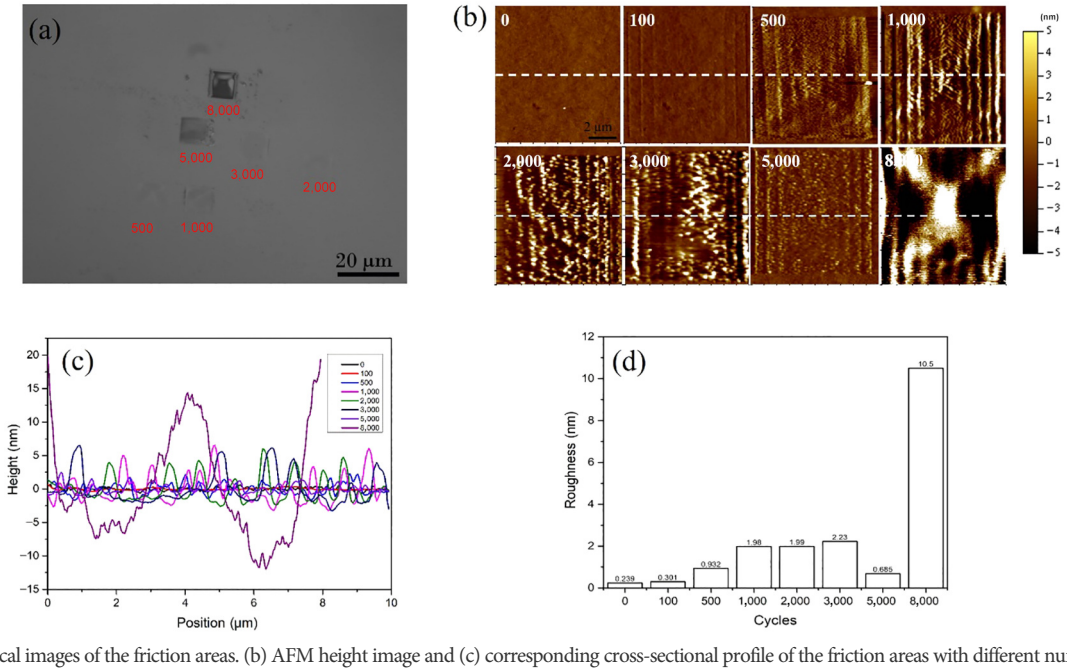

Fig. 2 (a) Optical images of the friction areas. (b) AFM height image and (c) corresponding cross-sectional profile of the friction areas with different numbers of sliding cycles. (d) Surface roughness obtained via AFM.

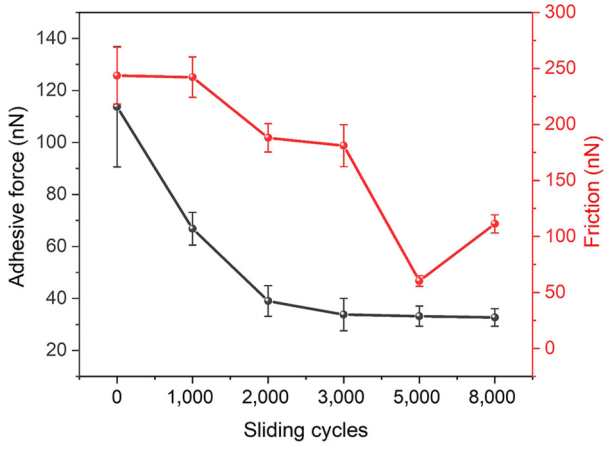

Fig. 3 Friction and adhesive forces between the protein film and the bare AFM tip plotted against the number of sliding cycles.

in surface roughness. The detailed chemical analysis is described in Section 3.3.

3.3 Chemical characterization

ToF-SIMS, a sensitive method used to identify the composition of surfaces, was used to explore the thickness and composition of the protein layer. Figure 4 shows the ToF-SIMS spectra and elemental maps of the wear areas. The 2D TOF-SIMS image of the wear areas (Fig. 4(a)) indicates that the brightness of the regions below 5,000 on the map was almost indistinguishable from that of the substrate, whereas the 5,000-cycle region and the center of the 8,000-cycle region were brighter than the substrate. In addition, a dark signal region was present at the periphery of the 8,000-cycle region. The brightness of the map was positively correlated with the content. As shown in Fig. 4(b), the peaks in the ToF-SIMS spectrum of the carbon-containing fragments (e.g., C^-, CH^-, C_2^-, and C_2H^-) in the 5,000-cycle sample were significantly greater

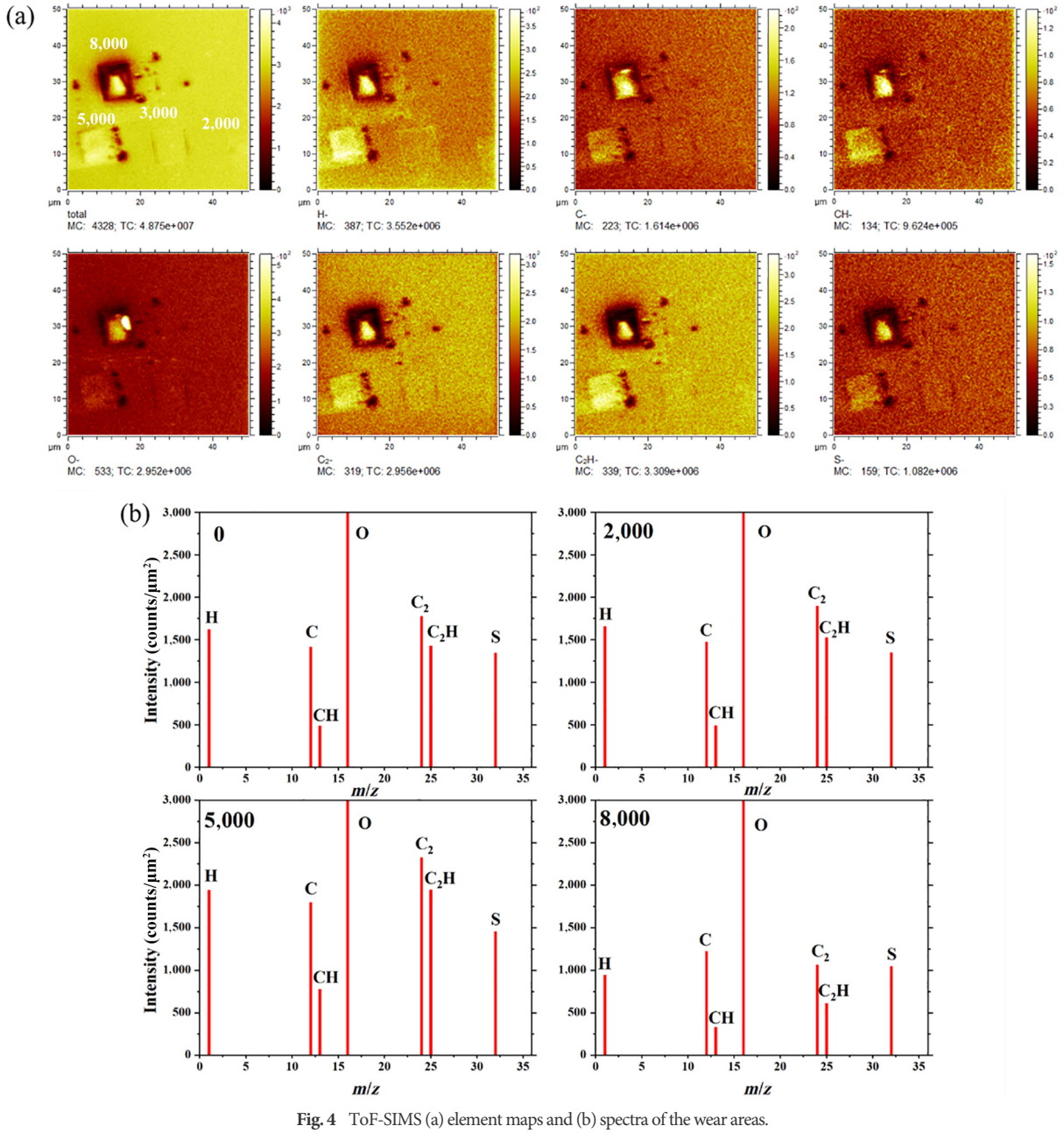

Fig. 4 ToF-SIMS (a) element maps and (b) spectra of the wear areas.

than the peaks in the remainder of the spectra, whereas the peaks in the 8,000-cycle sample were the lowest. The results shown in Fig. 4 indicate that more carbon and hydrocarbon debris formed in the 5,000- and 8,000-cycle regions.

To explore the composition evolution of proteins under shear force, ToF-SIMS depth profiling experiments were performed. Figures 5(a)–5(d) present the negative ion polarity depth profiles for the 0-, 2,000-, 5,000-, and 8,000-cycle regions. As shown in Fig. 5, the organic component signals (C^-, H^-, CH^-, C_2^-, S^-, and C_2H^-) undulated twice with depth in the 0-, 2,000-, and 5,000-cycle regions, whereas the signals undulated only once in the 8,000-cycle region. In contrast, the O^- signal continued to increase with depth, indicating the gradual exposure of the substrate. From these two signal trends, we divided the surface into a friction layer and a BSA layer, with the tribo-layer denoting the region of the outside protein layer that was denatured due to drying or friction, and the BSA layer denoting the unaffected portion inside the protein layer.

Figure 5(e) presents the thicknesses of the tribolayer and BSA layer in different sliding cycle areas. As shown in Fig. 5(e), the thicknesses of the tribolayers were 8.5, 8.5, 7.5, and 7.8 nm for 0, 2,000, 5,000, and 8,000 cycles, respectively. The thickness of the BSA layer was 5 nm after 0, 2,000, and 5,000 cycles, whereas the 8,000-cycle region did not contain a BSA layer due to excessive wear. The thickness information indicated that the wear of the protein layer started at cycle 5,000 and further intensified at cycle 8,000, which coincided with the compositional changes. During this process, the thickness of the tribolayer remained stable. This result indicates that protein denaturation under friction requires a long induction period. There is a transformation from the BSA layer to the tribo-layer during the wear process.

To further analyze the trends in various elemental changes between the different friction cycles, we compared four types of ion signals (C^-, H^-, S^-, and CH^-) in the depth range of the tribolayer (Fig. 6). As shown in the figure, the curves of each component between 0 and 2,000 cycles almost completely

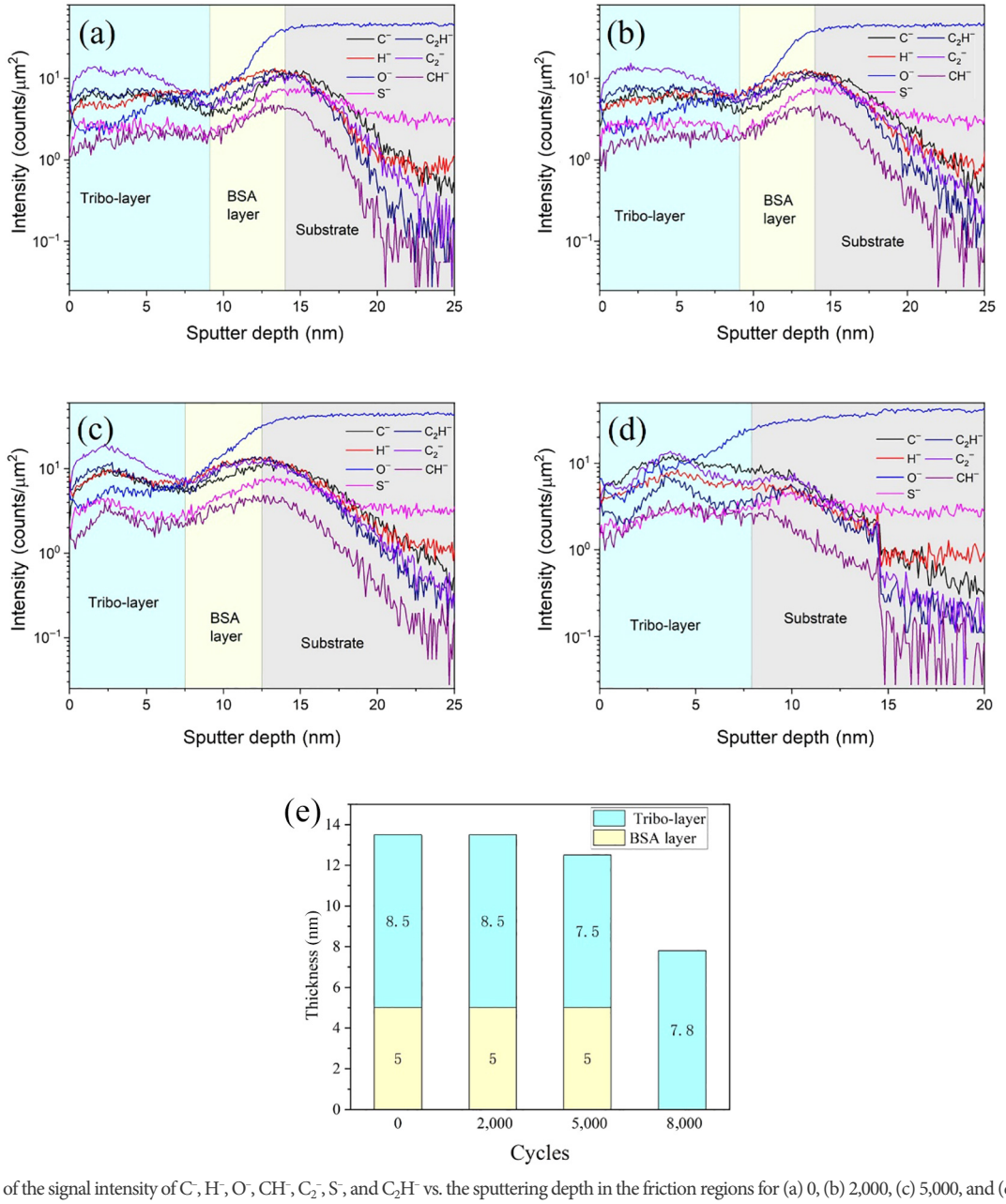

Fig. 5 Curves of the signal intensity of C^-, H^-, O^-, CH^-, C_2^-, S^-, and C_2H^- vs. the sputtering depth in the friction regions for (a) 0, (b) 2,000, (c) 5,000, and (d) 8,000 cycles.

清華大學出版社 Tsinghua University Press | SciOpen

overlapped, suggesting that the components did not change in the 2,000-cycle region. Compositional changes occurred mainly in the 5,000- and 8,000-cycle regions. Notably, the C^- signal was significantly greater after 5,000 and 8,000 cycles, and the trend was more pronounced after 8,000 cycles. For H^-, S^-, and CH^-, the content was significantly lower after 8,000 cycles than after 5,000 cycles, and the data suggested that dehydrogenation and desulfurization occurred between 5,000 and 8,000 cycles.

The micro-Raman spectra of the sliding regions were acquired to investigate the structure of the friction areas with different numbers of sliding cycles, as shown in Fig. 7(a). The spectroscopy data of all the regions revealed three main Raman bands for BSA, namely, the amide I band at 1,661 cm^{-1}, the CH_2 bending band at 1,450 cm^{-1}, and the C–H stretching band at 2,930 cm^{-1} [25–27]. The amide I band was attributed mainly to C=O stretching, C-N in-plane stretching, and N-H in-plane bending. The exact locations of these bands depend on the secondary structure of the peptide group, which can be used to predict the secondary structure of the protein [25]. The Raman spectroscopy results revealed that BSA molecules in friction areas primarily contained β-sheets and random curled structures. The Raman band at 1,450 cm^{-1} corresponded to the CH_2 bending band produced by the amino acids of the proteins, and their intensity reflected the amount of protein, which was insensitive to the local environment [26]. Therefore, the band at 1,450 cm^{-1} could be used as an internal standard for protein content, and its intensity was linearly proportional to the protein content. The intensity of the band at 1,450 cm^{-1} decreased in the 8,000-cycle region, which was consistent with the occurrence of wear. The band at 2,930 cm^{-1} corresponded to C–H stretching, and the increase in intensity at 2,930 cm^{-1} likely arose from the unfolding of the protein molecules and the increasing polarity of the environment of the

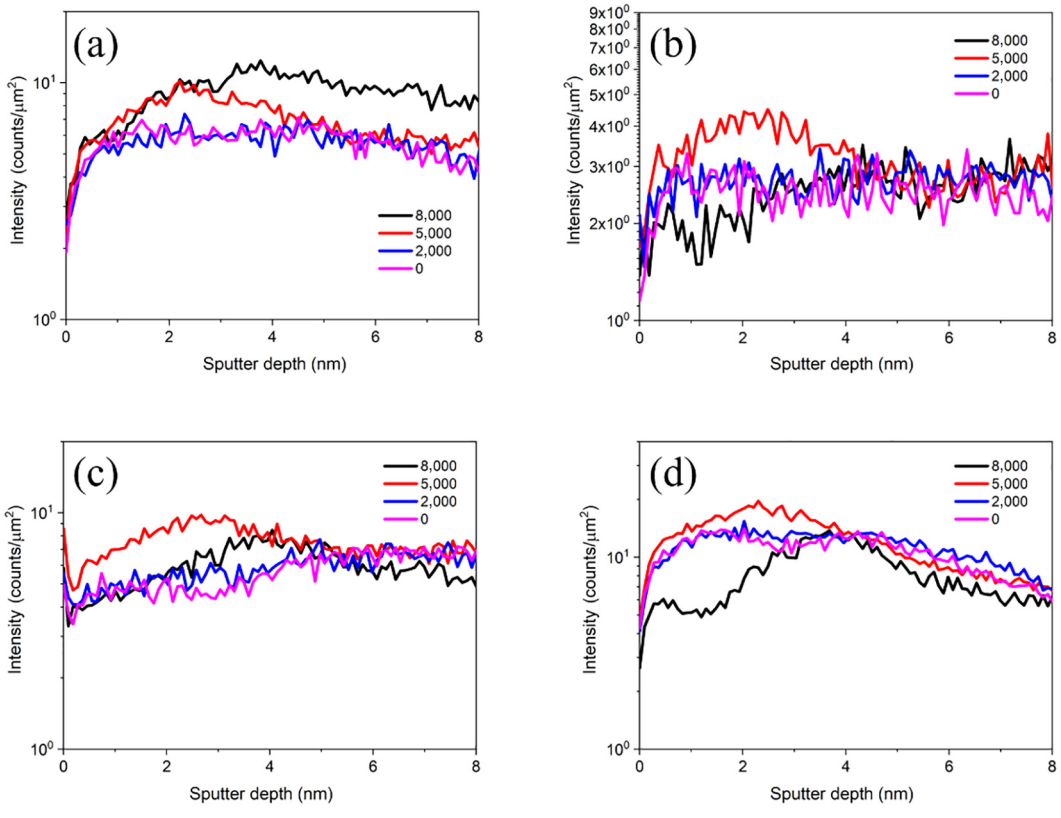

Fig. 6 Signal intensity curves of the different sliding cycle regions vs. the sputtering depth in the tribolayer for (a) C^-, (b) H^-, (c) S^-, and (d) CH^-.

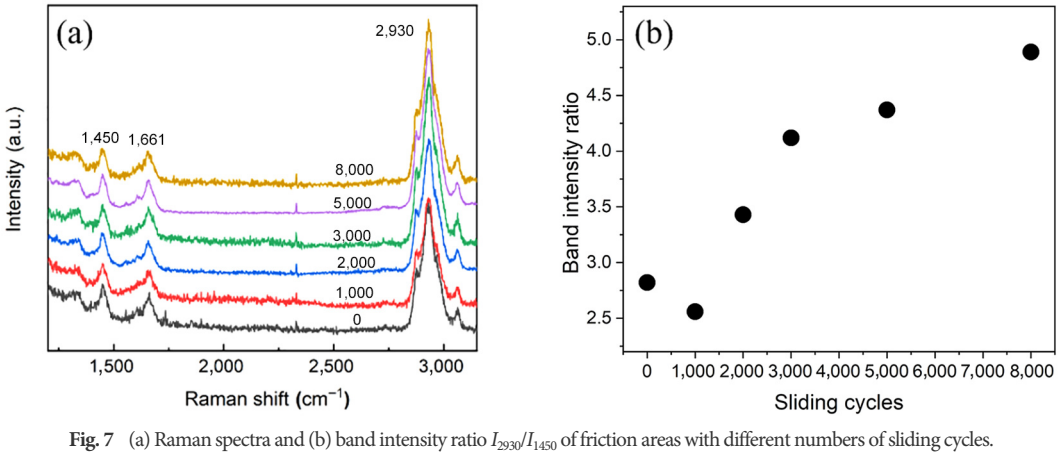

Fig. 7 (a) Raman spectra and (b) band intensity ratio I_{2930}/I_{1450} of friction areas with different numbers of sliding cycles.

CH_2 and CH_3 groups of the lipid hydrocarbon chains [27]. As shown in Fig. 7(b), the I_{2930}/I_{1450} band intensity ratio increased with increasing number of friction cycles, possibly indicating the unfolding of BSA molecules and the further formation of short-chain structures during friction.

The Raman spectroscopy data did not exhibit the characteristic peaks of graphitic structures in all regions, suggesting that shear alone was not sufficient to drive the graphitization transition of proteins. This process may require the combined action of other factors (transition metal catalysis) [16, 28, 29]. Figure 8 shows a schematic of the protein denaturation process under AFM tip friction. Under the shear force applied by the AFM probe, the protein adsorption layer undergoes spreading and wear, leading to protein breakage and dehydrogenation, and ultimately, a carbonaceous tribofilm can form on the surface. The formation of carbonaceous tribofilms can significantly reduce the friction force due to their low viscosity and high internal stiffness from C–C bonding [30].

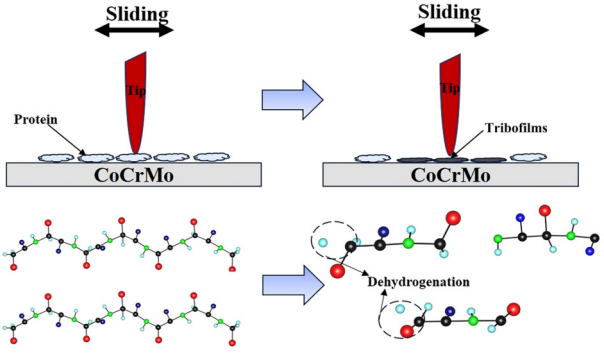

Fig. 8 Schematic of protein denaturation under AFM tip friction.

4 Conclusions

The changes in the composition and properties of protein layers under shear stress were investigated via a controlled atomic force microscopy (AFM) single-asperity sliding experiment. This study revealed that surface property and composition changes occurred with increasing number of sliding cycles. In the initial sliding stage, friction was affected mainly by adhesive forces, and with prolonged time, the generation and destruction of lubricating surfaces became the main influencing factors. Proteins first unfold under shear and then undergo chain breaking, dehydrogenation, and desulfurization over time as friction progresses. In addition, the carbonaceous fragments did not show graphitization under only shear stress.

Acknowledgements

This work was supported by the National Natural Science Foundation of China (No. 51971035).

Declaration of competing interest

The authors have no competing interests to declare that are relevant to the content of this article.

References

[1] Ferguson R J, Palmer A J R, Taylor A, Porter M L, Malchau H, Glyn-Jones S. Hip replacement. *Lancet* **392**(10158): 1662–1671 (2018)
[2] Katz J N, Winter A R, and Hawker G. Measures of the appropriateness of elective orthopedic joint and spine procedures. *Journal of Bone and Joint Surgery* **99**(4): e15 (2017)
[3] Koizumi Y, Chen Y, Li Y P, Yamanaka K, Chiba A, Tanaka S I, Hagiwara Y. Uneven damage on head and liner contact surfaces of a retrieved Co–Cr-based metal-on-metal hip joint bearing: An important reason for the high failure rate. *Mater Sci Eng C* **62**: 532–543 (2016)
[4] Tunthawiroon P, Li Y P, Chiba A. Influences of alloyed Si on the corrosion resistance of Co–Cr–Mo alloy to molten Al by iso-thermal oxidation in air. *Corros Sci* **100**: 428–434 (2015)
[5] Mathew M T, Runa M J, Laurent M, Jacobs J J, Rocha L A, Wimmer M A. Tribocorrosion behavior of CoCrMo alloy for hip prosthesis as a function of loads: A comparison between two testing systems. *Wear* **271**(9–10): 1210–1219 (2011)
[6] Yan Y. *Bio-Tribocorrosion in Biomaterials and Medical Implants*. London (UK): Woodhead Publishing Limited, 2013.
[7] Gallo J, Goodman S B, Konttinen Y T, Wimmer M A, Holinka M. Osteolysis around total knee arthroplasty: A review of pathogenetic mechanisms. *Acta Biomater* **9**(9): 8046–8058 (2013)
[8] Clarke M T, Lee P T H, Arora A, Villar R N. Levels of metal ions after small- and large-diameter metal-on-metal hip arthroplasty. *J Bone Jt Surg Br Vol* **85-B**(6): 913–917 (2003)
[9] Langton D J, Jameson S S, Joyce T J, Gandhi J N, Sidaginamale R, Mereddy P, Lord J, Nargol A V F. Accelerating failure rate of the ASR total hip replacement. *J Bone Jt Surg Br Vol* **93-B**(8): 1011–1016 (2011)
[10] Mihalko W M, Wimmer M A, Pacione C A, Laurent M P, Murphy R F, Rider C. How have alternative bearings and modularity affected revision rates in total hip arthroplasty. *Clin Orthop Relat Res* **472**(12): 3747–3758 (2014)
[11] Wimmer M A, Sprecher C, Hauert R, Täger G, Fischer A. Tribochemical reaction on metal-on-metal hip joint bearings. *Wear* **255**(7–12): 1007–1014 (2003)
[12] Wimmer M A, Fischer A, Büscher R, Pourzal R, Sprecher C, Hauert R, Jacobs J J. Wear mechanisms in metal-on-metal bearings: The importance of tribochemical reaction layers. *J Orthop Res* **28**(4): 436–443 (2010)
[13] Wang Z W, Yan Y, Su Y J, Qiao L J. Effect of electrochemical corrosion on the subsurface microstructure evolution of a CoCrMo alloy in albumin containing environment. *Appl Surf Sci* **406**: 319–329 (2017)
[14] Pourzal R, Theissmann R, Morlock M, Fischer A. Micro-structural alterations within different areas of articulating surfaces of a metal-on-metal hip resurfacing system. *Wear* **267**(5–8): 689–694 (2009)
[15] Yan Y, Neville A, Dowson D, Williams S, Fisher J. Tribofilm formation in biotribocorrosion–does it regulate ion release in metal-on-metal artificial hip joints. *P I Mech Eng Part J J Eng Tribol* **224**(9): 997–1006 (2010)
[16] Liao Y, Pourzal R, Wimmer M A, Jacobs J J, Fischer A, Marks L D. Graphitic tribological layers in metal-on-metal hip replacements. *Science* **334**(6063): 1687–1690 (2011)
[17] Hesketh J, Ward M, Dowson D, Neville A. The composition of tribofilms produced on metal-on-metal hip bearings. *Biomaterials* **35** (7): 2113–2119 (2014)
[18] Martin E J, Pourzal R, Mathew M T, Shull K R. Dominant role of molybdenum in the electrochemical deposition of biological macromolecules on metallic surfaces. *Langmuir* **29**(15): 4813–4822 (2013)
[19] Ghanbarzadeh A, Motamen Salehi F, Bryant M, Neville A. Modelling the evolution of electrochemical current in potentiostatic condition using an asperity-scale model of tribocorrosion. *Biotribology* **17**: 19–29 (2019)
[20] Bhushan B, Tokachichu D R, Keener M T, Lee S C. Nanoscale adhesion, friction and wear studies of biomolecules on silicon based surfaces. *Acta Biomater* **2**(1): 39–49 (2006)
[21] Sader J E, Chon J W M, Mulvaney P. Calibration of rectangular

atomic force microscope cantilevers. *Rev Sci Instrum* **70**(10): 3967–3969 (1999)
[22] Green C P, Lioe H, Cleveland J P, Proksch R, Mulvaney P, Sader J E. Normal and torsional spring constants of atomic force microscope cantilevers. *Rev Sci Instrum* **75**(6): 1988–1996 (2004)
[23] Butt H J, Cappella B, Kappl M. Force measurements with the atomic force microscope: Technique, interpretation and applications. *Surf Sci Rep* **59**(1–6): 1–152 (2005)
[24] Gosvami N N, Ma J, Carpick R W. An *in situ* method for simultaneous friction measurements and imaging of interfacial tribochemical film growth in lubricated contacts. *Tribol Lett* **66**(4): 154 (2018)
[25] Ota C, Takano K. Behavior of bovine serum albumin molecules in molecular crowding environments investigated by Raman spectroscopy. *Langmuir* **32**(29): 7372–7382 (2016)
[26] Wesełucha-Birczyńska A, Kozicki M, Czepiel J, Birczyńska M. Raman micro-spectroscopy tracing human lymphocyte activation. *Analyst* **138**(23): 7157 (2013)
[27] Howell N K, Arteaga G, Nakai S, Li-Chan E C Y. Raman spectral analysis in the C–H stretching region of proteins and amino acids for investigation of hydrophobic interactions. *J Agric Food Chem* **47**(3): 924–933 (1999)
[28] Deng Q Y, Feng Q G, Jing P P, Ma D L, Li M T, Gong Y L, Li Y T, Wen F, Leng Y X. Metal-driven autoantifriction function of artificial hip joint. *Adv Sci* **10**(25): 2301095 (2023)
[29] Erdemir A, Ramirez G, Eryilmaz O L, Narayanan B, Liao Y F, Kamath G, Sankaranarayanan S K R S. Carbon-based tribofilms from lubricating oils. *Nature* **536**(7614): 67–71 (2016)
[30] Zhai W Z, Zhou K. Nanomaterials in superlubricity. *Adv Funct Mater* **29**(28): 1806395 (2019)

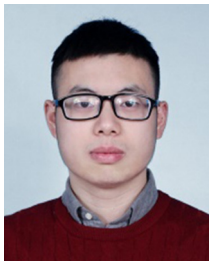

Jiachen Chen received his bachelor degree in material science from Jiangsu University, China, in 2016. He is studying for his Ph.D. degree at the University of Science and Technology Beijing, China. His research focused mainly on tribochemical films and biotribocorrosion.

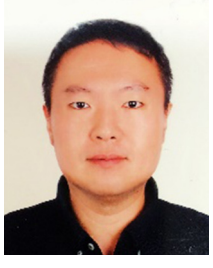

Yu Yan is a fellow of the Institute of Physics, CEng, Ph.D. He received his Ph.D. degree from the University of Leeds, UK, under the supervision of Prof. Anne Neville and Prof. Duncan Dowson. He has published over 150 papers, and he focuses on the interaction of tribological contact and corrosion reactions in biological environments.